J Nanopart Res (2010) 12:2967–2978
DOI 10.1007/s11051-010-9887-4

RESEARCH PAPER

Surfactant-modified nickel zinc iron oxide/polymer nanocomposites for radio frequency applications

Ta-I. Yang · Rene N. C. Brown · Leo C. Kempel · Peter Kofinas

Received: 11 November 2009 / Accepted: 20 February 2010 / Published online: 12 March 2010
© Springer Science+Business Media B.V. 2010

Abstract Low loss, flexible, polymer nanocomposites with improved magneto-dielectric properties at radio frequencies (RF) were successfully fabricated. Surfactant-modified nickel zinc iron oxide ($NiZnFe_2O_4$) nanoparticles with ferrimagnetic behavior at room temperature were synthesized by a seed-mediated growth method. The surfactant prevented $NiZnFe_2O_4$ particle aggregation and provided compatibility with [styrene-b-ethylene/butylene-b-styrene] block copolymer matrices. $NiZnFe_2O_4$/polymer composites were prepared by a solution-casting method. Experimental results showed that the dielectric permittivity (ε_r) and magnetic permeability (μ_r) of the polymer composite increased with increasing amount of $NiZnFe_2O_4$ doping. The dielectric loss ($\tan\delta$) was less than 0.010 at 1 GHz frequency. The increased miniaturization factor ($(\varepsilon_r\mu_r)^{1/2}$) and relative wave impedance ($(\mu_r/\varepsilon_r)^{1/2}$) of the $NiZnFe_2O_4$ nanocomposites could potentially lead to a reduced RF device's physical size with ease in impedance matching. Dynamic mechanical analysis (DMA) revealed that nanocomposites maintained 125% strain (elongation at break) with 30% nanoparticle doping.

Keywords Nickel zinc iron oxide · Polymer composite · Magneto-dielectric · Magnetic nanoparticle · Nanocomposites

T.-I. Yang · P. Kofinas (✉)
Fischell Department of Bioengineering, University of Maryland, College Park, MD 20742, USA
e-mail: kofinas@umd.edu

R. N. C. Brown
Department of Chemical and Biomolecular Engineering, University of Maryland, College Park, MD 20742, USA

L. C. Kempel
Department of Electrical and Computer Engineering, Michigan State University, East Lansing, MI 48824, USA

Introduction

Radio frequency (RF) nanocomposites with tailored magneto-dielectric properties are promising for advanced applications in microwave communication and radar systems. Smaller physical size, wider operating bandwidth, and higher power efficiency are desired characteristics. For antenna applications, the miniaturization factor and wave impedance (η) are proportional to the square-root of the product and ratio of the relative permeability (μ_r) and relative dielectric permittivity (ε_r), respectively (Buerkle and Sarabandi 2005; Mosallaei and Sarabandi 2004). This means that for a higher value of μ_r or ε_r, a smaller antenna can be obtained and with a higher ratio of μ_r to ε_r, a wider bandwidth with ease in impedance matching will be available. Most importantly, the materials should possess low dielectric loss tangent ($\tan\delta$) to ensure higher power efficiency. Polymer/particle composites possess greater advantages over purely ceramic

materials due to their ease in processing and applicability to conformal installations. Various magnetic particle/polymer composites have been developed for microwave antenna applications. The most common method to fabricate these composites is to blend inorganic particles into polymers (Gupta et al. 2005; Koulouridis et al. 2006; Shirakata et al. 2008; Yashchyshyn and Modelski 2005). Such methods lack control on particle characteristic length (size and shape) and distribution within the polymer matrix, which are critical factors affecting the magnetic properties of the composites.

In this study, we demonstrate the feasibility of preparing flexible nickel zinc iron oxide (NZFO)/polymer nanocomposites with improved miniaturization factor and wave impedance (η) in the radio frequency (RF) range. The reason for utilizing NZFO nanoparticles is their superior properties, such as high resistivity, high permeability, and low dielectric loss in microwave device applications (von Aulock et al. 1965; Pardavi-Horvath 2000). Surface-modified NZFO nanoparticles were synthesized using a sodium oleate surfactant to improve compatibility with the polymer matrix (Cushing et al. 2004). The size of the nanoparticles was tailored by a seed-mediated method, which utilizes smaller nanoparticles as growth sites to synthesize larger particles. The size and shape of individual particles were able to be quantified compared to highly aggregated nanoparticles synthesized using co-precipitation (Majewski et al. 2008; Rao et al. 2007), sol–gel auto-combustion (Zhang et al. 2007), or micelle techniques (Uskokovic et al. 2004; Yan and Zhou 2005). The dielectric (ε_r) and magnetic (μ_r) properties of the resulting nanocomposites consisting of various nanoparticles dispersed in polymer matrices were measured using impedance analysis.

Experimental section

Materials

Sodium oleate (97%) was purchased from TCI America. Iron chloride ($FeCl_3$, 97%), nickel chloride ($NiCl_2$, 98%), zinc chloride ($ZnCl_2$, 99.99%), oleic acid (90%), and 1-octadecene (90%) were purchased from Sigma-Aldrich. The block copolymer of [styrene-b-ethylene/butylene-b-styrene] (SEBS) was supplied by Kraton Polymers. All chemicals were used as received.

Synthesis of 13.2 ± 3.8 nm (Generation 1) and high Zn-containing $NiZnFe_2O_4$ nanoparticles

For the preparation of Generation 1 nanoparticles, $FeCl_3$ (24 mmol, 3.89 g), $NiCl_2$ (6 mmol, 0.78 g), $ZnCl_2$ (6 mmol, 0.82 g), and sodium oleate (96 mmol, 29.2 g) were reacted in a mixed solvent (80 mL ethanol, 60 mL distilled water, and 140 mL hexane) at 70 °C for 4 h. The upper organic layer containing the ion–surfactant complex (NiZnFe precursor) was washed thrice with 30 mL distilled water and then dried. The resulting complex was added into 200 mL of 1-octadecene mixed with oleic acid (5.6 g). The mixture was heated to 320 °C in an argon atmosphere. After 30 min at 320 °C, the solution turned black, and was then cooled down to room temperature. Ethanol was added to precipitate the surfactant-coated nickel zinc iron oxide ($NiZnFe_2O_4$) particles. The precipitated particles were centrifuged to remove any residual solvent. For the synthesis of high Zn-containing $NiZnFe_2O_4$ nanoparticles, the procedure was the same as with Generation 1 particles with the exception of the chemical composition of NiZnFe precursor and the addition of seeds in the 1-octadecene solution. The NiZnFe precursor was prepared using $FeCl_3$ (24 mmol, 3.89 g), $NiCl_2$ (3 mmol, 0.38 g), and $ZnCl_2$ (9 mmol, 1.22 g). The seeds were 2 g of as-synthesized Generation 1 particles.

Synthesis of seed-mediated growth $NiZnFe_2O_4$ nanoparticles (Generations 1 and 2)

The procedure was the same as with the synthesis of 13.2 ± 3.8 nm Generation 1 $NiZnFe_2O_4$ particles except the addition of 2 g seeds. The seeds used to generate Generation 2 (17.3 ± 5.6 nm) and Generation 3 particles (16.1 ± 9.2 nm) were as-synthesized Generation 1 and 2 particles, respectively.

Preparation of $NiZnFe_2O_4$ nanocomposites

The $NiZnFe_2O_4$/polymer nanocomposites were prepared by a solution-casting method, since both surfactant-modified $NiZnFe_2O_4$ nanoparticles and polymer matrices dissolve in a common solvent, tetrahydrofuran (Schallibaum et al. 2009). In a typical formulation, 1.5 g of SEBS polymer in 40 mL THF was mixed with the desired amount of $NiZnFe_2O_4$ nanoparticles (1.08 g for 30 wt% and 0.36g for 14

wt%). The resultant solution was mixed by an overhead stirrer for 1 h to obtain a homogenous solution. The solution was subsequently poured into a Teflon dish and a film of 0.2 mm thickness was cast over a period of one day.

Characterization

Transmission electron microscopy (TEM, JEOL 200CX) was used to observe the morphology of the nanoparticles. Samples for TEM were prepared by evaporating a dilute $NiZnFe_2O_4$ THF solution on a carbon-coated grid. The particle size is reported as the average observed size (D_{avg}), which is the average particle size of approximately 1,000 individual particles from multiple TEM images. Magnetic properties were investigated using a vibrating sample magnetometer (VSM, Lakeshore 7400 series). The powder X-ray diffraction measurements (XRD) of the samples were conducted on a Bruker C2 Discover and D8 Advance systems using Cu Kα ($\lambda = 0.154$ nm) radiation. The crystallite size (D_{XRD}) of the synthesized nanoparticles was measured using the Scherrer formula (Cullity 1965).

$$D_{XRD} = \frac{0.9\lambda}{B\cos\theta} \quad (1)$$

where λ is the X-ray wavelength, the width B is measured at an intensity equal to half the maximum intensity, and θ is the Bragg angle.

X-ray photoelectron spectroscopy (XPS, Kratos AXIS 165) was used to investigate the oxidation state of nickel, zinc, and iron. The charge-shifted spectra were corrected assuming that the adventitious C 1*s* peak detected was at 284.600 eV. Scanning electron microscope (SEM) images were obtained using a Hitachi SU-70 microscope operating at 20 kV. Energy dispersive X-ray spectroscopy (EDS) equipped within SEM was used to determined the chemical composition of the synthesized nanoparticles. Tensile strength and ultimate elongation were studied with a dynamic mechanical analyzer (DMA, TA Instruments Q800). The amount of NZFO within the polymer matrix was determined using thermogravimetric analysis (TGA, Shimadzu TGA-50) in nitrogen atmosphere. The polymer and surfactant were removed, and only NZFO particles remained without change in crystalline structure. The magneto-dielectric properties (relative dielectric permittivity ε_r and relative magnetic permeability μ_r) in the 1MHz–1GHz range were measured using an Agilent RF impedance/material analyzer (E4991A). Samples for ε_r measurement were prepared in the shape of a solid disc with a diameter of 0.75 inch and a thickness of 0.1 inch. Samples for μ_r measurement were in the geometry of a washer with an outer diameter of 0.75 inch, an empty inner diameter of 0.25 inch, and a thickness of 0.1 inch. Multiple measurements (at least five times) were obtained and their standard deviations were calculated.

Results and discussion

Surface-modified NZFO nanoparticles

Seed synthesis

In the classic LaMer mechanism (Watzky and Finke 1997), the formation of colloids from homogenous solution occurs when the precursor concentration is above the supersaturated limit. Further growth of nuclei is spontaneous, but limited by diffusion of the precursor to the nucleus surface. In our nanoparticle synthesis system, iron, nickel, and zinc ions were released by dissociation from the ion–surfactant complex (NiZnFe precursor) at 320 °C (Park et al. 2004). The released metallic ions subsequently nucleated as new nanoparticle seeds (path I in Fig. 1) or diffused to the seed surface and grew into bigger particles (path II in Fig. 1). The resultant nanoparticles (Generation 1) synthesized from decomposition of (Ni,Zn,Fe)–surfactant complex were non-spherical with average size (D_{avg}) of 13.2 ± 3.8 nm, as shown in Fig. 2. The narrow particle size distribution suggests that most particles grew from the formed nucleus at the same time. There is limited new particle nucleation during the particle growth phase. The electron diffraction pattern from the TEM image shows multiple diffraction rings (left inset of Fig. 2), indicating crystalline structure formation. The nanoparticles were highly soluble in organic solvents (THF or hexane) and no aggregation between particles was observed in TEM images. This indicated that the surface of the nanoparticles was modified by the oleic acid surfactant. The bulky hydrophobic part of the surfactant provides nanoparticle solubility in organic solvents and also the steric isolation needed to prevent van der Waals attraction and magnetic attraction

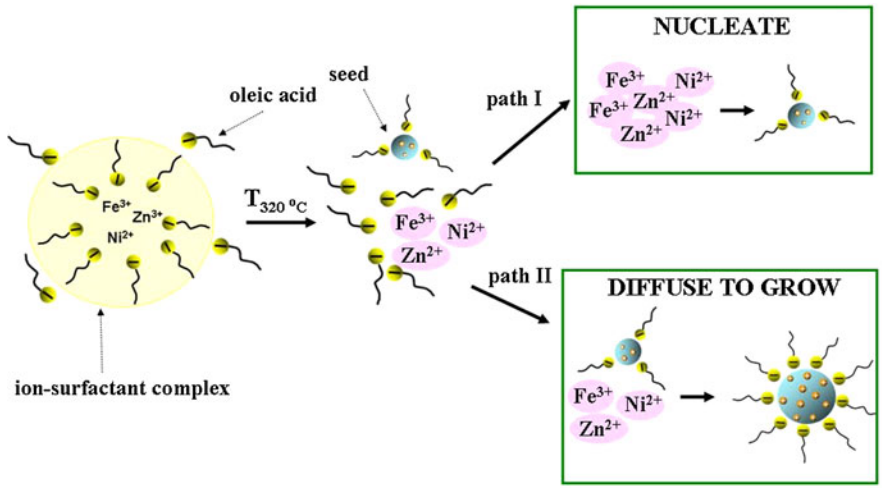

Fig. 1 Scheme depicting nucleation and growth of nanoparticles from the ion–surfactant complex

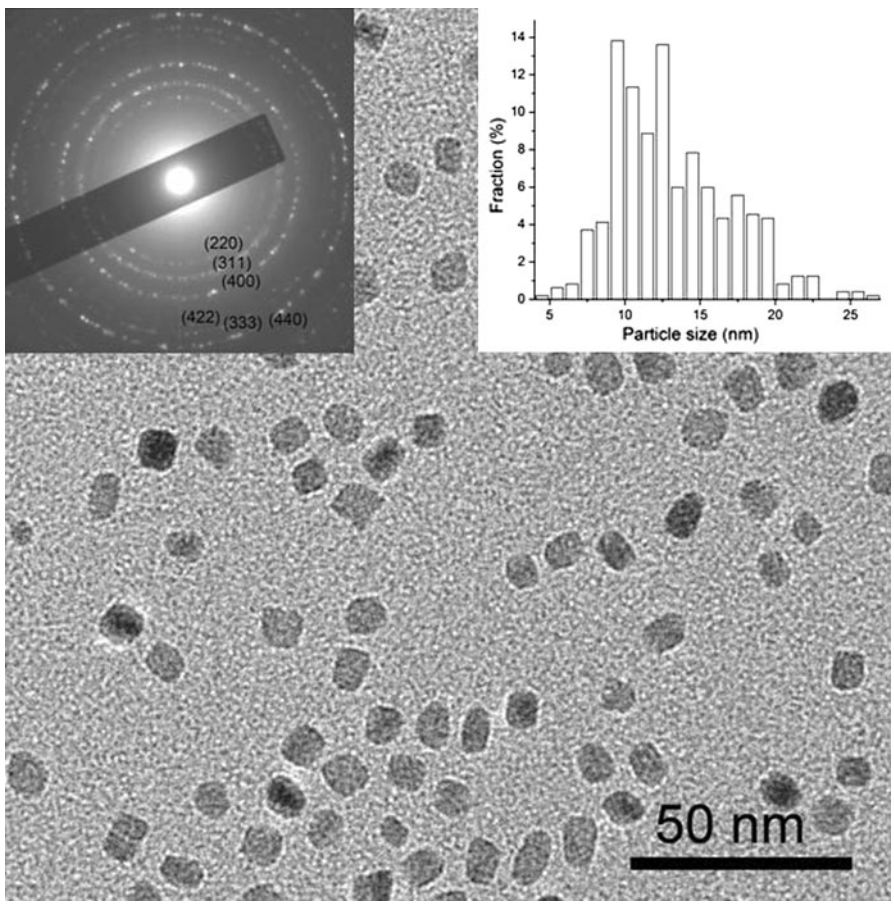

Fig. 2 TEM image of 13.2 ± 3.8 nm $NiZnFe_2O_4$ nanoparticles (Generation 1; *left inset*: selected area electron diffraction; *right inset*: particle size distribution)

among magnetic particles. Fourier transform infrared (FTIR) was utilized to confirm that the surface of synthesized nanoparticles was coated with surfactants (oleic acid), as shown in Fig. 3. The broad feature between 3,500 and 2,500 cm^{-1} is due to the O–H stretch of the carboxylic acid groups of oleic acid. Two sharp bands at 2,914 and 2,847 cm^{-1} are attributed to the asymmetric CH_2 stretch and the

symmetric CH_2 stretch, respectively. The bands at 1,560 and 1,463 cm^{-1} are characteristic of the asymmetric $v_{as}(COO^-)$ and symmetric $v_s(COO^-)$ stretch, which confirm that oleic acid is chemisorbed as a carboxylate onto the nanoparticle surface as previously reported in literature (Wu et al. 2004).

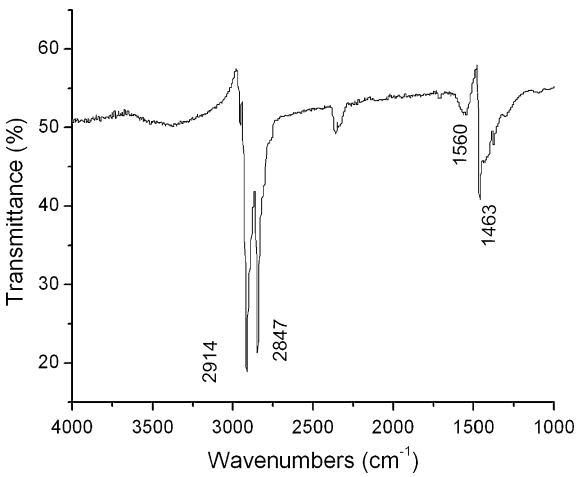

Fig. 3 FTIR spectroscopy spectrum of surface-modified nanoparticles

Seed-mediated growth

Larger surface-modified nanoparticles can be obtained by a seed-mediated method, where the original synthesized nanoparticle seeds are used as nuclei to grow larger particles. Figure 4 confirmed that larger 17.3 ± 5.6 nm nanoparticles (Generation 2) can be synthesized using Generation 1 particles (13.2 ± 3.8 nm) as growth seeds. However, these nanoparticles have broader size distribution compared to the narrower size distribution of seeds added, as shown on the right inset of Fig. 4. This result could be attributed to the fact that both nucleation and growth steps are prevalent during nanoparticle formation. The released metallic ions not only diffused to the seed surface and then grew into bigger particles (path II in Fig. 1) but also nucleated as new nanoparticles (path I in Fig. 1). It

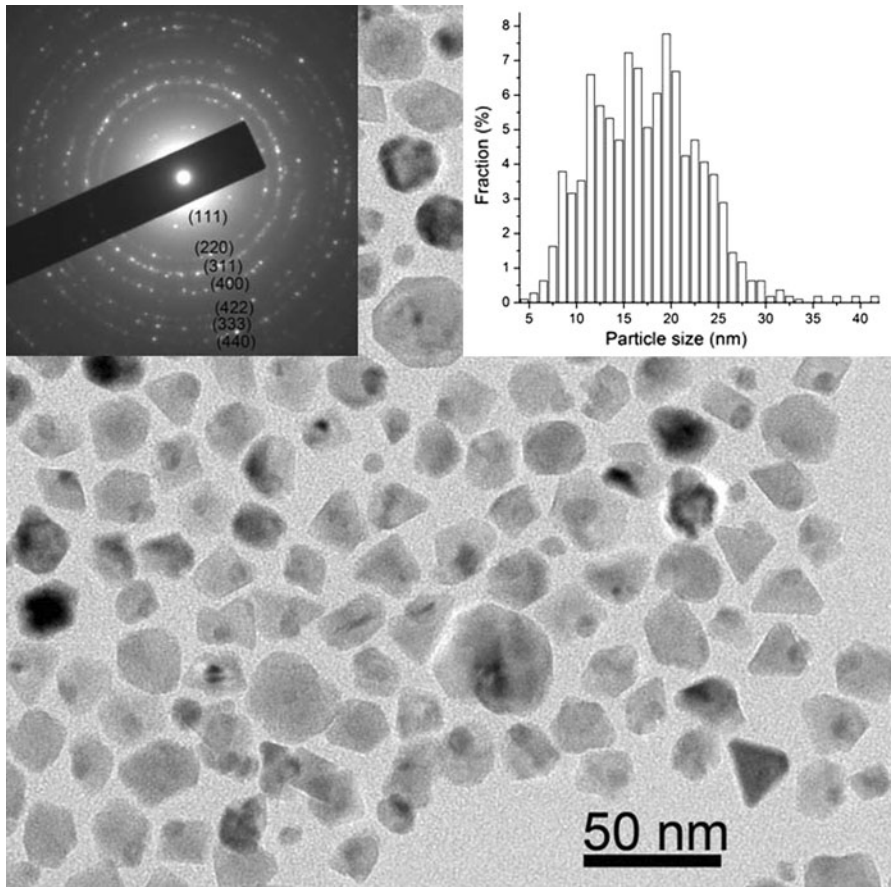

Fig. 4 TEM image of 17.3 ± 5.6 nm $NiZnFe_2O_4$ nanoparticles (Generation 2; *left inset*: selected area electron diffraction; *right inset*: particle size distribution)

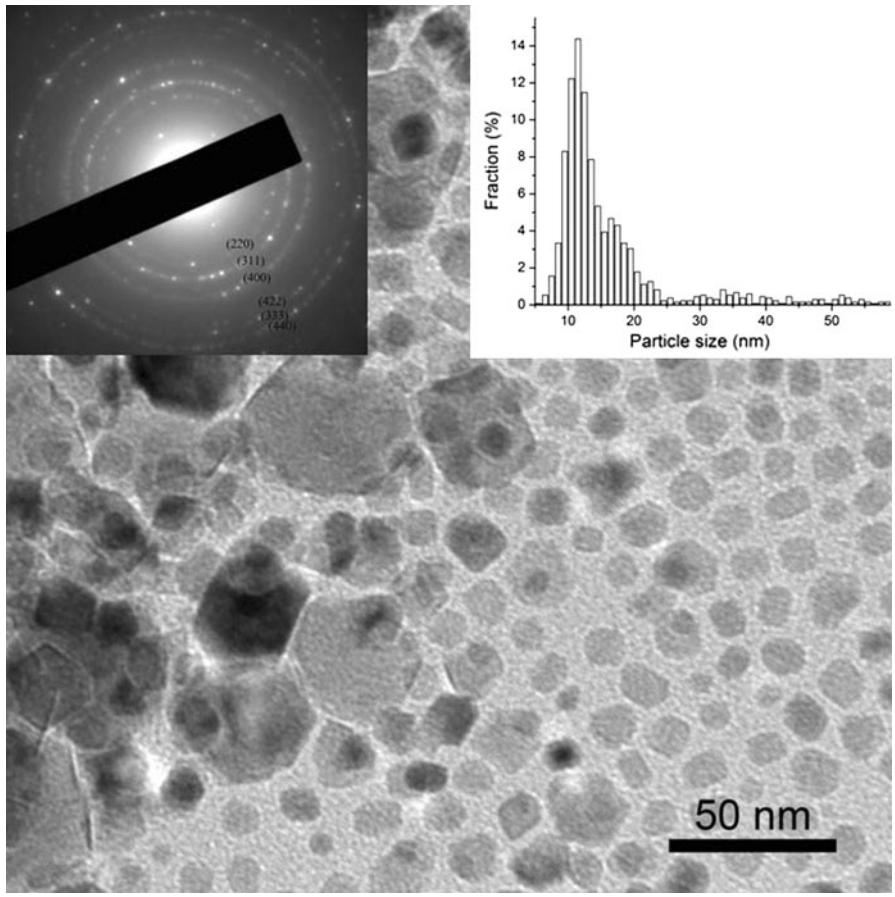

Fig. 5 TEM image of 16.1 ± 9.2 nm $NiZnFe_2O_4$ nanoparticles (Generation 3; *left inset*: selected area electron diffraction; *right inset*: particle size distribution)

is believed that particles with size smaller and larger than ~16 nm originate from the nucleation of new particles and from the growth of the added seeds, respectively, since 90% of seeds are smaller than 16 nm.

Figure 5 also shows that smaller nanoparticles with a broader particle size distribution (16.1 ± 9.2 nm) can be synthesized with the same conditions as Generation 2 particles (17.3 ± 5.6 nm), except using Generation 2 particles as the seeds. The average size of 16.1 nm does not correctly represent the size of these Generation 3 particles since their size distribution is highly polydisperse. It is obvious that these nanoparticles composed of nanoparticles grown from newly formed nuclei and from the Generation 2 particles as well. These results further confirm that neither the nucleation nor the growth step dominated during nanoparticle formation.

In summary, larger surface-modified nanoparticles could be obtained by a seed-mediated method. However, larger seeds did not lead to larger particles as evidenced by comparing the size distribution of synthesized nanoparticles seeded with different particle sizes (Fig. 6). It is clear even larger particles are achievable from Generation 2 to Generation 3 particles, since particles could grow from seeds. However, the nucleation process still occurs at the same time during particle growth. Therefore, not only all the released metal ions diffuse to the seed surface to grow but also instead nucleate into new particles. It is necessary to impede the nucleation process to grow larger particles.

Chemical structure

Structural information of the synthesized nanoparticles was obtained from both TEM selected area electron diffraction (SAED) and wide angle X-ray diffraction (XRD). The SAED patterns from the left insets of Figs. 2, 4, and 5 show multiple diffraction rings. The calculated lattice *d*-spacings derived from the diffraction rings are 4.83, 2.98, 2.53, 2.10, 1.71,

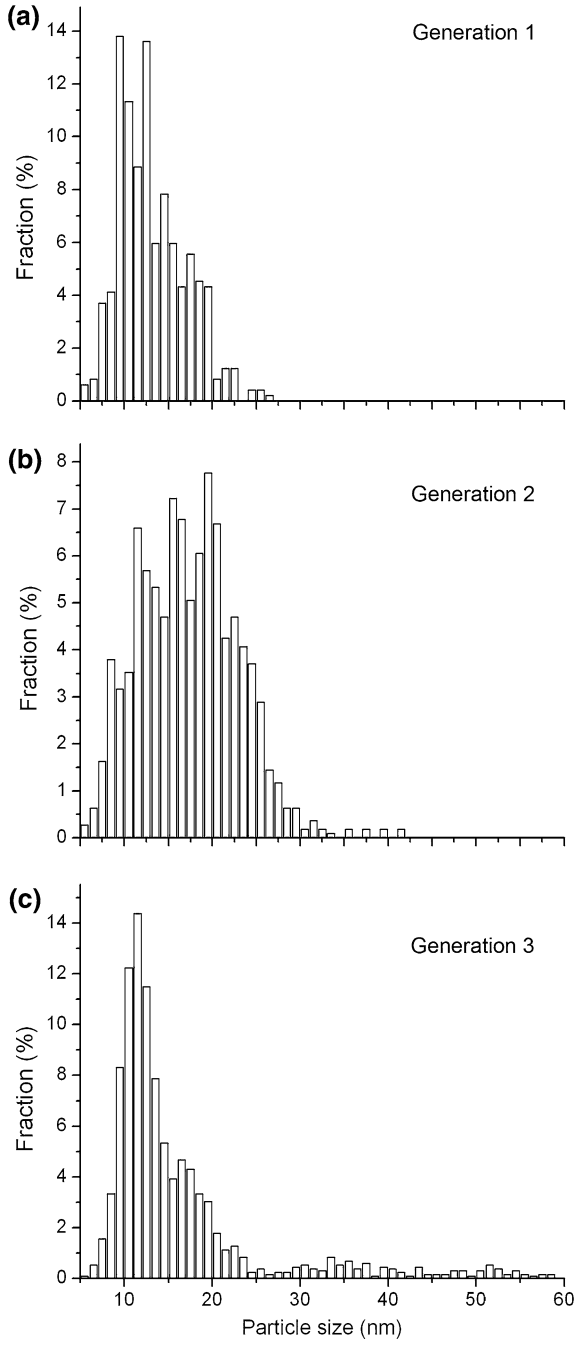

Fig. 6 Particle size distribution of synthesized nanoparticles with different seeding conditions

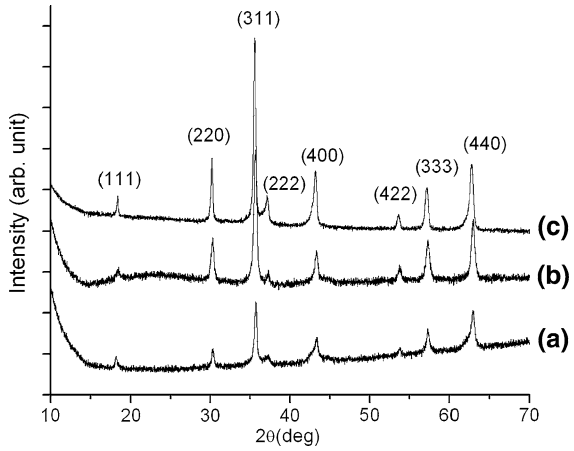

Fig. 7 Wide angle X-ray diffraction pattern of synthesized $NiZnFe_2O_4$ nanoparticles. **a** Generation 1; **b** Generation 2; **c** Generation 3

1.60, and 1.48 Å corresponding to (111), (220), (222), (400), (422), (333), and (440) planes of $NiZnFe_2O_4$, respectively. Figure 7 shows XRD patterns of synthesized nanoparticles. The positions of all diffraction rings/peaks are consistent with standard $NiZnFe_2O_4$ powder diffraction data reported in literature (JCPDS 1991) and no other metal oxides, such as ZnO or NiO or α-Fe_2O_3, could be identified. In addition to the crystalline structure, the crystallite size of synthesized nanoparticles could be obtained from their XRD peaks using Scherrer's formula. The calculated average crystallite size (D_{XRD}) for Generation 1 particles is 13 nm, consistent with the size obtained from TEM images. However, the D_{XRD} for Generation 2 particles is 22 nm, which is larger than the size from D_{avg} (17.3 $\pm$ 5.6 nm). For the Generation 3 particles, the difference between D_{avg} (16.1 $\pm$ 9.2 nm) and D_{XRD} (25nm) is even larger. This is because larger particles contribute more to the diffraction measurement when compared to smaller particles (Cullity 1965). High-resolution XPS was utilized to determine the oxidation state of the nanoparticles, and is shown in Fig. 8. The binding energies of Fe $2p_{3/2}$ (710.4 eV), Ni $2p_{3/2}$ (854.8 eV), and Zn $2p_{3/2}$ (1,022.2 eV) are in agreement with existing literature, and are characteristic of $NiZnFe_2O_4$ (Hayashimto et al. 2007). Energy dispersive X-ray spectroscopy (EDS) revealed the chemical compositions of synthesized nanoparticles (Table 1). EDS showed that the Generation 1 particles (13.2 $\pm$ 3.8 nm) composed of higher stoichiometric amounts of nickel compared to zinc, although there is an equal amount of both metals within the starting ion–surfactant complex. The Generation 2 particles (17.3 $\pm$ 5.6 nm) synthesized through seeding showed even higher stoichiometric amounts of nickel. These

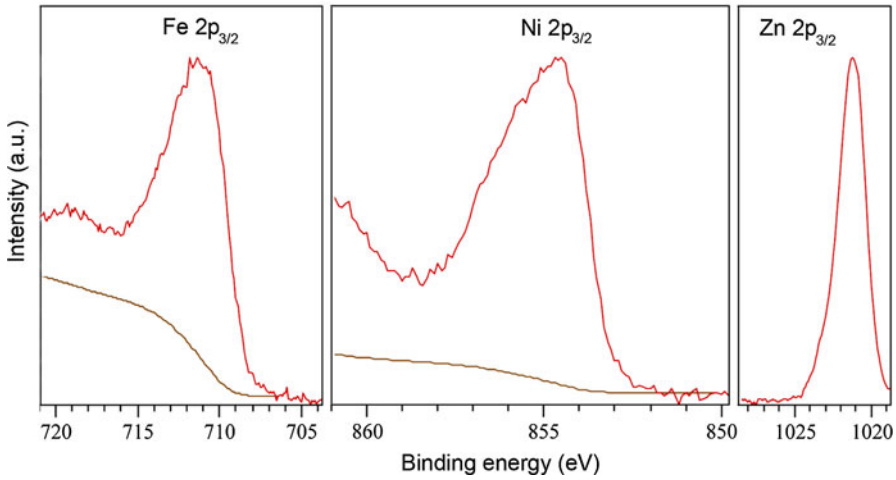

Fig. 8 XPS spectra of synthesized $NiZnFe_2O_4$ nanoparticles (Generation 1)

Table 1 EDS data of synthesized nanoparticles (unit: atom %)

Sample	Fe	Ni	Zn
Generation 1	68	18	14
Generation 2	72	19	9
High Zn-containing	71	15	14

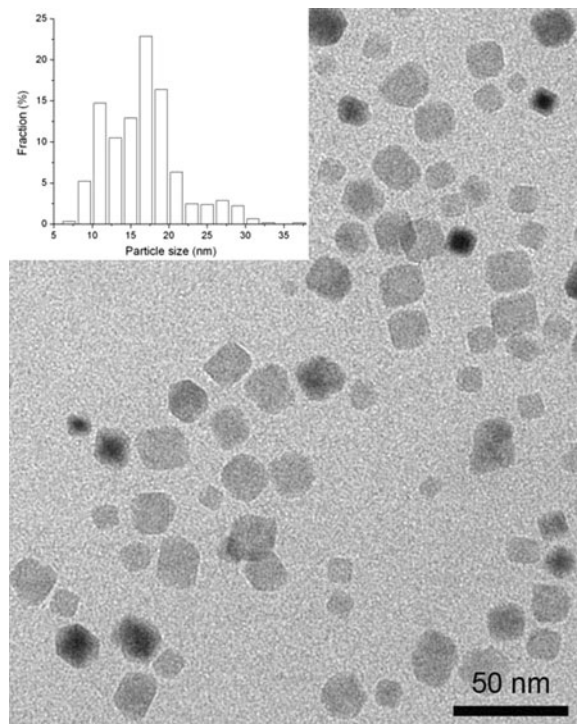

Fig. 9 High Zn-containing NZIO nanoparticles (*inset*: particle size distribution)

results indicated that during nanoparticle formation the zinc atom is kinetically less favorable to fit into the nanoparticle crystalline structure than nickel and iron do. In order to further confirm the kinetic hypothesis of zinc ions contributing to particle formation, ion–surfactant complexes with higher zinc amount were used to prepare the $NiZnFe_2O_4$ nanoparticles. The synthesis procedure was the same as with the synthesis of Generation 2 particles except using ion–surfactant complex with richer amount of zinc (mole ratio of zinc to nickel was 3). The size of the resultant nanoparticles was 16.6 ± 4.8 nm close to Generation 2 particles (17.3 ± 5.6 nm), as shown in Fig. 9. An equal amount of zinc and nickel was measured in these synthesized nanoparticles (Table 1). This result proves that the ion–surfactant complex precursor should contain higher zinc concentration to result in $NiZnFe_2O_4$ nanoparticles with higher zinc amount, since the reaction kinetic for $NiZnFe_2O_4$ formation is proportional to initial precursor concentrations.

Magnetic properties of $NiZnFe_2O_4$ nanoparticles

Figure 10 shows the room temperature magnetization as a function of applied magnetic field for Generation 1 (13.2 ± 3.8 nm), Generation 2 (17.3 ± 5.6 nm), and Generation 3 (16.1 ± 9.2 nm) $NiZnFe_2O_4$ nanoparticles. The $NiZnFe_2O_4$ nanoparticles with average particle size of 13.2 ± 3.8 nm show typical superparamagnetic behavior: In the absence of hysteresis with both values of coercivity and remanence being zero. However, there is hysteresis present for the 17.3 ± 5.6 nm particles (Generation 2) with a

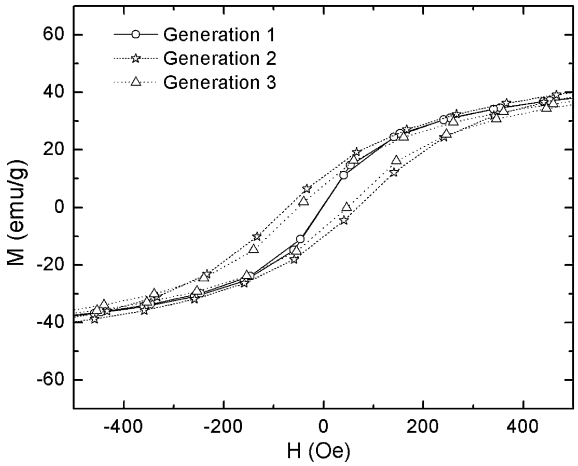

Fig. 10 Magnetization (M) versus applied magnetic field (H) for Generations 1, 2, and 3 $NiZnFe_2O_4$ nanoparticles

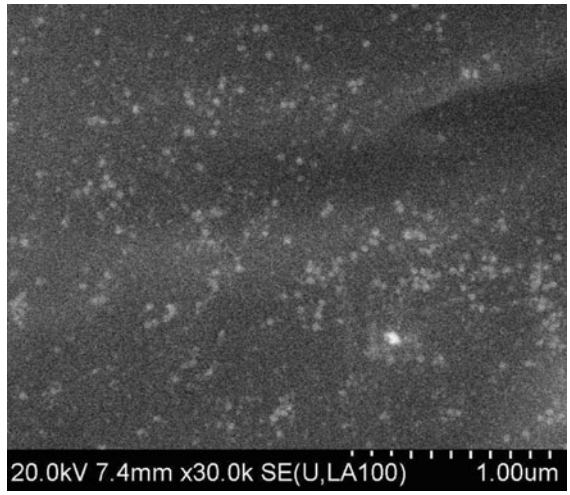

Fig. 11 SEM image of polymer nanocomposites with 30 wt% of Generation 2 $NiZnFe_2O_4$ nanoparticles

coercivity (H_c) of 70 Oe, which is consistent with ferrimagnetic behavior. It has been reported in literature that the $NiZnFe_2O_4$ critical size (D_{SP}) for superparamagnetic to ferrimagnetic transition is close to 20 nm (Burukhin et al. 2001). Therefore, the 17.3 ± 5.6 nm nanoparticles (Generation 2) approximately comprise of 68% superparamagnetic and 32% ferrimagnetic particles according to the histogram in Fig. 4. Generation 3 (16.1 ± 9.2 nm) nanoparticles also exhibited ferrimagnetic behavior with a coercivity (H_c) of 65 Oe and approximately comprise of 84% superparamagnetic and 16% ferrimagnetic particles according to the histogram in Fig. 5. It was also observed that the saturation magnetization (M_s) of these $NiZnFe_2O_4$ nanoparticles (Generations 1,2, and 3) is lower than the bulk value of $NiZnFe_2O_4$ (73 emu/g) due to spin disorder and cation redistributions arising from the larger particle surface area (smaller particles), as reported in literature (Goya et al. 2003; Rao et al. 2007; Swaminathan et al. 2005; Zhang et al. 2007).

Magneto-dielectric and mechanical properties of the $NiZnFe_2O_4$/polymer composites

Ferrimagnetic Generation 2 (17.3 ± 5.6 nm) instead of superparamagnetic Generation 1 (13.2 ± 3.8 nm) $NiZnFe_2O_4$ nanoparticles were chosen to prepare polymer composites. This is because larger particles result in higher anisotropy energies (KV) required to maintain the particle's magnetization and obtain higher values of magnetic permeability (μ_r; Yang et al. 2008). The $NiZnFe_2O_4$/polymer nanocomposites were prepared by a solution-casting method, since both surfactant-modified $NiZnFe_2O_4$ nanoparticles and polymer matrices dissolve in a common solvent, such as tetrahydrofuran. The $NiZnFe_2O_4$ nanoparticles dispersed well in the SEBS polymer matrix without any severe particle aggregation, although some $NiZnFe_2O_4$ clusters appeared due to magnetic attraction between particles as shown in Fig. 11. The resultant relative dielectric permittivity (ε_r) and magnetic permeability (μ_r) of the polymer nanocomposites prepared by a simple solution-casting method are shown in Fig. 12. The relative permittivity of the [styrene-b-ethylene/butylene-b-styrene] (SEBS) copolymer ($\varepsilon_r = 2.4$) improved from 2.4 to 2.9 with increasing amount of $NiZnFe_2O_4$ nanoparticles. The dielectric loss (tanδ) was less than 0.010 at the 1 GHz frequency range as shown in Fig. 13. The magnetic permeability of the SEBS copolymer ($\mu_r = 1$) also improved from 1.0 to 1.4 at 1 GHz with increasing amounts of $NiZnFe_2O_4$ nanoparticle doping. Accordingly, an increased miniaturization factor $((\varepsilon_r\mu_r)^{0.5})$ and improved relative wave impedance $(\eta/\eta_0 = (\mu_r/\varepsilon_r)^{0.5})$ of the $NiZnFe_2O_4$ nanocomposites can also be obtained with increasing amount of $NiZnFe_2O_4$ nanoparticles as shown in Table 2 (η_0 is the wave impedance of free space, 377 Ω). In theory, the antenna size is proportional to $1/(\varepsilon_r\mu_r)^{0.5}$ (Buerkle and Sarabandi 2005). Higher

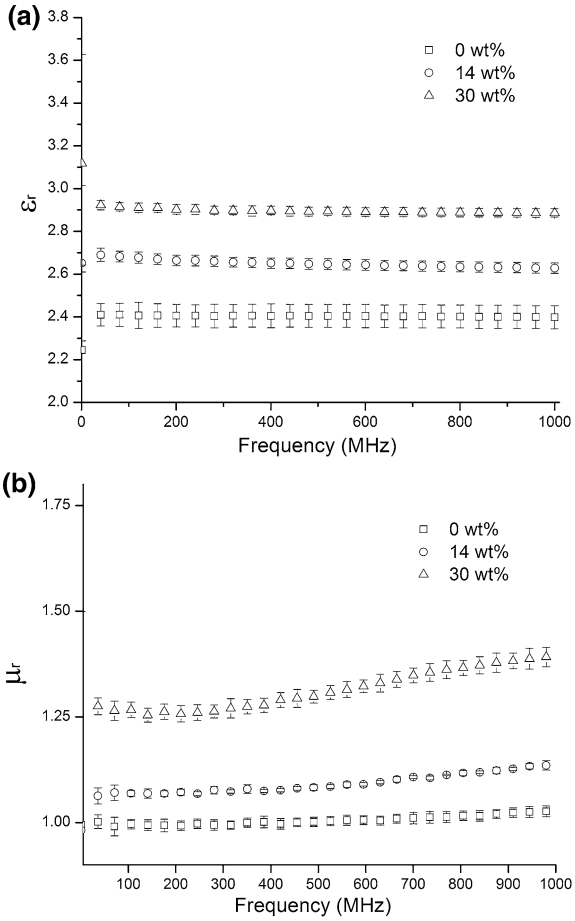

Fig. 12 **a** Relative dielectric permittivity and **b** relative magnetic permeability of surfactant-modified $NiZnFe_2O_4$ nanocomposites

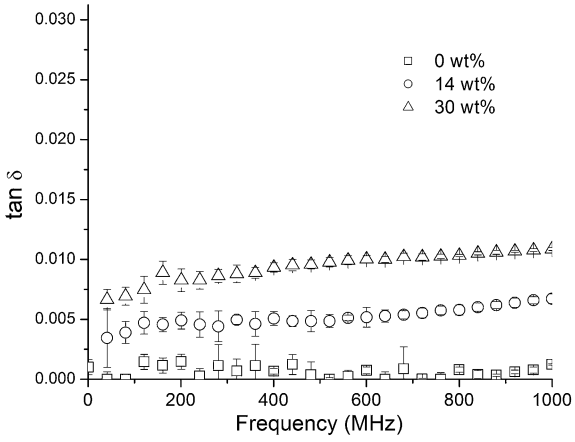

Fig. 13 Dielectric loss (tanδ) of surfactant-modified $NiZnFe_2O_4$ nanocomposites

Table 2 Dielectric permittivity, magnetic permeability, miniaturization factor ($(\varepsilon_r\mu_r)^{1/2}$), and relative wave impedance ($(\mu_r/\varepsilon_r)^{1/2}$) at 1 GHz frequency for polymer composites with various weight percentages (wt%) of $NiZnFe_2O_4$ nanoparticle doping

wt%	ε_r	μ_r	$(\varepsilon_r\mu_r)^{1/2}$	$(\mu_r/\varepsilon_r)^{1/2}$
0	2.4	1.0	1.55	0.63
14	2.6	1.1	1.69	0.65
30	2.9	1.4	2.01	0.69

Note: The relative wave impedance is the impedance ratio of composite to free space

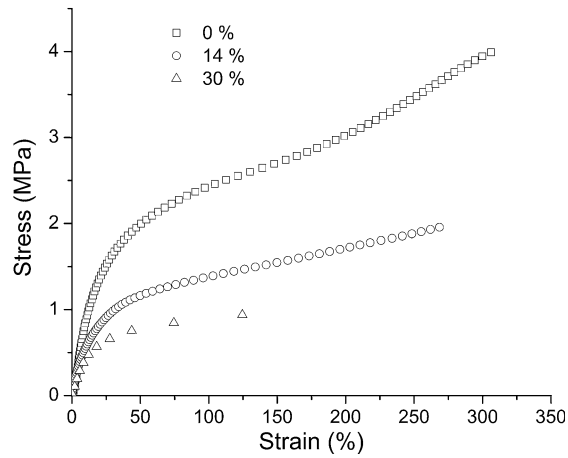

Fig. 14 Mechanical stress/strain curves of polymer nanocomposites with various $NiZnFe_2O_4$ nanoparticle wt%

values of miniaturization factor enable a smaller antenna size. Also, it is easy to do impedance matching on an antenna when the relative wave impedance (η/η_0) is close to 1. Therefore, a smaller antenna with ease in impedance matching can be achieved by utilizing polymer composites doped with surfactant-modified $NiZnFe_2O_4$ nanoparticles.

Dynamic mechanical analysis (DMA) was used to evaluate the tensile strength and ultimate elongation of the SEBS composites containing $NiZnFe_2O_4$ nanoparticles. Controlled force stress–strain experiments were performed to obtain the stress–strain curve shown in Fig. 14. Compared to the pure SEBS block copolymer, the ultimate elongation and tensile strength of the composites decreased with increasing amounts of $NiZnFe_2O_4$ nanoparticle doping. This is because the nanoparticle/surfactant complex serves as a plasticizer to reduce the integrity and strength of the

composites (Denver et al. 2007). However, the composites still maintained 125% strain with 30% nanoparticle doping, indicating the highly flexible nature of the fabricated nanocomposites.

Conclusions

We have demonstrated the feasibility of preparing low loss, flexible polymer nanocomposites with improved magneto-dielectric properties at radio frequencies. Surfactant-modified nickel zinc iron oxide ($NiZnFe_2O_4$) nanoparticles were synthesized using smaller nanoparticles as growth sites to obtain larger particles of various target sizes. Polymer nanocomposites were prepared by a solution-casting method. The dielectric permittivity and magnetic permeability of the composites increased by adding surfactant-modified $NiZnFe_2O_4$ nanoparticles. The increased miniaturization factor and wave impedance of the $NiZnFe_2O_4$ nanocomposites at 1 GHz frequency show promise for significantly miniaturizing the physical size of microwave communication devices, with ease in impedance matching.

Acknowledgements This article is based upon study supported by the Air Force Office of Scientific Research, Grant # FA95500910430. We also acknowledge the support of the Maryland NanoCenter and its NispLab. The NispLab is supported in part by the NSF as a MRSEC Shared Experimental Facility.

References

Buerkle A, Sarabandi K (2005) A wide-band, circularly polarized, magnetodielectric resonator antenna. IEEE Trans Antennas Propag 53:3436–3442

Burukhin AA, Churagulov BR, Oleinikov NN, Meskin PE (2001) Synthesis of nanosized ferrite powders from hydrothermal and supercritical solutions. Russ J Inorg Chem 46:646–651

Cullity BD (1965) Elements of X-ray diffraction. Addison-Wesley, Reading, MA

Cushing BL, Kolesnichenko VL, O'Connor CJ (2004) Recent advances in the liquid-phase syntheses of inorganic nanoparticles. Chem Rev 104:3893–3946

Denver H, Hong J, Borca-Tasciuc DA (2007) Fabrication and characterization of nickel nanowire polymer composites. Mater Res Soc Symp Proc 963:0963-Q20-60

Goya GF, Berquo TS, Fonseca FC, Morales MP (2003) Static and dynamic magnetic properties of spherical magnetite nanoparticles. J Appl Phys 94:3520–3528

Gupta N, Kashyap SC, Dube DC (2005) Microwave behavior of substituted lithium ferrite composites in X-band. J Magn Magn Mater 288:307–314

Hayashimto Y, Sakamoto W, Yogoa T (2007) Synthesis of nickel zinc ferrite nanoparticle/organic hybrid from metalorganics. J Mater Res 22:1967–1974

JCPDS—International Centre for Diffraction Data (1991) Powder diffraction file alphabetical index. Swarthmore, PA, USA, pattern# 08-234

Koulouridis S, Kiziltas G, Zhou YJ, Hansford DJ, Volakis JL (2006) Polymer-ceramic composites for microwave applications: fabrication and performance assessment. IEEE Trans Microw Theory Tech 54:4202–4208

Majewski P, Krysinski P (2008) Synthesis, surface modifications, and size-sorting of mixed nickel-zinc ferrite colloidal magnetic nanoparticles. Chem Eur J 14:7961–7968

Mosallaei H, Sarabandi K (2004) Magneto-dielectrics in electromagnetics: concept and applications. IEEE Trans Antennas Propag 52:1558–1567

Pardavi-Horvath M (2000) Microwave applications of soft ferrites. J Magn Magn Mater 215:171–183

Park J, An KJ, Hwang YS, Park JG, Noh HJ, Kim JY, Park JH, Hwang NM, Hyeon T (2004) Ultra-large-scale syntheses of monodisperse nanocrystals. Nat Mater 3:891–895

Rao BP, Rao GSN, Kumar AM, Rao KH, Murthy YLN, Hong SM, Kim CO, Kim C (2007) Soft chemical synthesis and characterization of $Ni_{0.65}Zn_{0.35}Fe_2O_4$ nanoparticles. J Appl Phys 101:123902

Schallibaum J, Torre FHD, Caseri WR, Loffler JF (2009) Large-scale synthesis of defined cobalt nanoparticles and magnetic metal–polymer composites. Nanoscale 1:374–381

Shirakata Y, Hidaka N, Ishitsuka M, Teramoto A, Ohmi T (2008) High permeability and low loss Ni–Fe composite material for high-frequency applications. IEEE Trans Magn 44:2100–2106

Swaminathan R, McHenry ME, Poddar P, Srikanth H (2005) Magnetic properties of polydisperse and monodisperse NiZn ferrite nanoparticles interpreted in a surface structure model. J Appl Phys 97:10G104

Uskokovic V, Drofenik M, Ban I (2004) The characterization of nanosized nickel-zinc ferrites synthesized within reverse micelles of CTAB/1-hexanol/water microemulsion. J Magn Magn Mater 284:294–302

von Aulock WH, Boxer AS, Ollom JF, Rauchmiller RF (1965) Handbook of microwave ferrite materials. Academic Press, New York

Watzky MA, Finke RG (1997) Transition metal nanocluster formation kinetic and mechanistic studies. A new mechanism when hydrogen is the reductant: slow, continuous nucleation and fast autocatalytic surface growth. J Am Chem Soc 119:10382–10400

Wu NQ, Fu L, Su M, Aslam M, Wong KC, Dravid VP (2004) Interaction of fatty acid monolayers with cobalt nanoparticles. Nano Lett 4:383–386

Yan SF, Zhou EL (2005) Transmission electron microscopy observation of the microemulsion process and the magnetic properties of the resultant nanocrystalline Ni-Zn ferrites. J Mater Res 20:2627–2631

Yang TI, Brown RNC, Kempel LC, Kofinas P (2008) Magneto-dielectric properties of polymer-Fe_3O_4 nanocomposites. J Magn Magn Mater 320:2714–2720

Yashchyshyn Y, Modelski JW (2005) Rigorous analysis and investigations of the scan antennas on a ferroelectric substrate. IEEE Trans Microw Theory 53: 427–438

Zhang HE, Zhang BF, Wang GF, Dong XH, Gao Y (2007) The structure and magnetic properties of $Zn_{1-x}Ni_xFe_2O_4$ ferrite nanoparticles prepared by sol–gel auto-combustion. J Magn Magn Mater 312:126–130